Two-dimensional solitons in the Gross-Pitaevskii equation with spatially modulated nonlinearity

Hidetsugu Sakaguchi[1] and Boris A. Malomed[2]
[1]*Department of Applied Science for Electronics and Materials, Interdisciplinary Graduate School of Engineering Sciences, Kyushu University, Kasuga, Fukuoka 816-8580, Japan*
[2]*Department of Interdisciplinary Studies, School of Electrical Engineering, Faculty of Engineering, Tel Aviv University, Tel Aviv 69978, Israel*
(Received 15 November 2005; published 2 February 2006)

We introduce a dynamical model of a Bose-Einstein condensate based on the two-dimensional Gross-Pitaevskii equation, in which the nonlinear coefficient is a function of radius. The model describes a situation with spatial modulation of the negative atomic scattering length, via the Feshbach resonance controlled by a properly shaped magnetic of optical field. We focus on the configuration with the nonlinear coefficient different from zero in a circle or annulus, including the case of a narrow ring. Two-dimensional axisymmetric solitons are found in a numerical form, and also by means of a variational approximation; for an infinitely narrow ring, the soliton is found in an exact form (in the latter case, exact solitons are also found in a two-component model). A stability region for the solitons is identified by means of numerical and analytical methods. In particular, if the nonlinearity is supported on the annulus, the upper stability border is determined by azimuthal perturbations; the stability region disappears if the ratio of the inner and outer radii of the annulus exceeds a critical value ≈ 0.47. The model gives rise to bistability, as the stationary solitons coexist with stable axisymmetric breathers, whose stability region extends to higher values of the norm than that of the static solitons. The collapse threshold strongly increases with the radius of the inner hole of the annulus. Vortex solitons are found too, but they are unstable.

DOI: 10.1103/PhysRevE.73.026601 PACS number(s): 05.45.Yv, 03.75.Lm, 42.65.Tg

I. INTRODUCTION

Matter-wave solitons have been created in Bose-Einstein condensates (BECs) in various effectively one-dimensional (1D) settings. First, these were dark solitons in repulsive condensates [1]. Then, bright solitons were created in an attractive BEC (lithium) [2]. This was followed by the making of gap solitons in a repulsive rubidium condensate loaded in a periodic potential, which was induced by the optical lattice (OL), i.e., interference pattern between two laser beams illuminating the medium [3].

A challenge to the experiment is creation of 2D matter-wave solitons. A natural problem in this case is the trend of solitons in multidimensional attractive condensates to be unstable because of the possibility of collapse in this setting [4]. In theoretical works, several approaches were proposed to stabilize 2D solitons. One of them uses a full two-dimensional OL [5], or its low-dimensional (quasi-1D) counterpart [6], which can stabilize fundamental solitons. In addition, 2D lattices lend stability to vortical solitons [5], including higher-order vortices, and "supervortex" complexes [7]; the latter ones are built as circular chains of compact vortices, with global vorticity imprinted onto the chain. Another theoretically elaborated approach relies upon the use of a nonlocal anisotropic nonlinearity induced by the long-range interactions between atoms with a magnetic momentum (chromium), polarized by an external field [8].

An alternative mechanism proposed for the stabilization of 2D matter-wave solitons is based on the Feshbach resonance (FR), which makes it possible to control the value of the scattering length, i.e., as a matter of fact, an effective nonlinear coefficient in the corresponding Gross-Pitaevskii equation (GPE), by means of an external magnetic field [9]. Moreover, the FR may switch the sign of the nonlinearity (in particular, the FR-induced switch from repulsion to weak attraction was instrumental to the creation of bright solitons in lithium [2]). Application of a low-frequency ac magnetic field may provide for periodic alternation of the nonlinearity sign in the GPE via the FR. It was predicted that the FR technique based on the ac field gives rise to novel states in the 1D geometry [10], and can stabilize 2D solitons, even in the absence of the external trap [11]. The same technique, if applied in combination with a quasi-1D OL potential, may also stabilize matter-wave solitons in the 3D geometry [12].

It has been predicted [13], and demonstrated in experiment [14], that the FR can also be induced by a properly tuned optical field. Then, illuminating the condensate by two counterpropagating coherent laser beams, one can build an OL that will provide for periodic modulation of the nonlinearity coefficient along the respective spatial coordinate. Solitons in the corresponding one-dimensional GPE with the nonlinear OL were recently investigated in Ref. [15], where stability regions for static solitons and breathers were found (motion of free solitons in the same model was recently studied in Ref. [16], and rigorous proofs concerning the stability of static solutions in this setting were reported in Ref. [17]). The soliton dynamics in the 1D model with other configurations of the spatial modulation of the nonlinearity coefficient was studied in Ref. [18] (unlike Ref. [15], the nonlinearity coefficient did not change its sign in the models considered in the latter works). It is relevant to mention that, in addition to the magnetic and optical fields, the strength of collisions between atoms in an ultracold gas may also be controlled by external dc electric field [19].

Static spatial modulation of the nonlinearity through the FR, controlled by a properly shaped external field, may be

tried as another means for the stabilization of 2D solitons, which is the subject of the present work. A natural form of an axisymmetric OL in the 2D geometry corresponds to the Bessel beam, i.e., a nondiffracting light signal in a bulk linear medium. In the case when the Bessel beam creates an effective linear potential in the equation of the GPE type with self-attraction, it has been shown that the corresponding radial lattice can readily stabilize various types of 2D solitons [20]. However, our results show that, within a broad parameter region that we were able to explore, stabilization of 2D solitons by means of a nonlinear Bessel lattice, i.e., within the framework of the GPE whose nonlinear coefficient is $g(r)=g_0J_n(ar)$, where r is the radial coordinate, g_0 and a are constants, and J_n is the Bessel function with $n=0,1,\ldots$, appears to be impossible—stationary axisymmetric soliton solutions can be easily constructed, but in simulations they all suffer either decay or collapse.

Nevertheless, in this work we demonstrate that a simpler shape of the radial modulation of the nonlinearity, in which it takes a constant value, corresponding to self-attraction, inside a finite circle or annulus, and is zero (or corresponds to self-repulsion) outside this region, is able to stabilize axisymmetric 2D solitons. In addition to that, we will demonstrate that the model gives rise to bistability: the stationary solitons coexist with stable breathers, that feature persistent oscillations in the radial direction. In fact, the stability region of the breathers is larger than that of the static solitons, extending to higher values of the norm (number of atoms in the BEC).

It should be said that, in the case of the nonlinearity controlled by the optical beam through the FR mechanism, the beam with the cross section in the form of a circle or annulus is not divergence-free, unlike its Bessel-shaped counterpart. However, this circumstance does not impede the physical realization of the model, as an effectively 2D condensate can be easily trapped between two blue-detuned light sheets, which strongly repel the atoms, as demonstrated in the experiment [21]. The thickness of the corresponding "pancake" is a few microns, while its diameter is measured in hundreds of microns (at least), hence the diffraction of the light beam within this range is completely negligible.

All the above was said about single-component BECs. Binary ultracold Bose gases, in the form of a mixture of two different hyperfine states of the same atomic species (rubidium) [22,23], as well as different species (potassium and rubidium) [24], have been created too. Various patterns and their stability in binary BECs were investigated theoretically [25–28], including bright solitons [29,30]. The FR may be used to control the interspecies scattering length in binary condensates too [31]. A possibility to stabilize a 2D vectorial (two-component) soliton by means of the FR in the low-frequency ac magnetic field, similar to how is was predicted for the single-component soliton [11], was considered in Ref. [32].

The paper is organized as follows. In Sec. II, we formulate the model, and present numerical and analytical solutions for static solitons. The analytical part includes a variational approximation for the solutions in the general case, an exact solution for solitons supported by an infinitely narrow annulus carrying the nonlinearity, and predictions for the stability against radial perturbations, based on the Vakhitov-Kolokolov (VK) [33,34] criterion. Exact solutions are also found for two-component solitons sustained by an infinitely narrow nonlinearity ring in the model of a binary BEC. The stability threshold for azimuthal perturbations (in the single-component model) is determined by a solution of the corresponding eigenvalue problem. An inference is that stability borders in the model with the nonlinearity supported on the circle are completely determined by radial perturbations, while in the annular model the upper stability border (in terms of the soliton's norm) is controlled by azimuthal perturbations. No stable solitons are possible if the annulus is relatively narrow, with the ratio of inner and outer radii exceeding a critical value ≈ 0.47. In Sec. III, we summarize results of direct numerical simulations of the stability of fundamental stationary solutions, which precisely confirm the existence of a well-defined stability region of the 2D solitons in the model's parameter space, predicted in Sec. II. The bistability (coexistence of the stable stationary solitons and breathers) and the extended stability region for the breathers are also reported in Sec. III. In Sec. IV, we briefly consider solitons with intrinsic vorticity, and conclude that all the vortices are unstable (the vortex splits in two fundamental solitons, each one then collapsing intrinsically). The paper is concluded by Sec. V.

II. STATIONARY SOLITONS

A. The model and numerical solutions

The GPE for the single-atom wave function ψ in the normalized form is

$$i\frac{\partial \psi}{\partial t} = -\frac{1}{2}\nabla^2\psi - g(r)|\psi|^2\psi, \tag{1}$$

with t time, ∇^2 the 2D Laplacian, and the nonlinearity coefficient shaped, by means of the external magnetic or optical field, as said above

$$g(r) = \begin{cases} 1, & \rho < r < R, \\ 0, & r < \rho \text{ or } r > R. \end{cases} \tag{2}$$

The number of atoms is determined by the norm of the wave function

$$N = 2\pi \int_0^\infty |\psi(r)|^2 r dr. \tag{3}$$

Using the scaling invariance of Eq. (1), we set $R=2$, keeping ρ as a free parameter. Note that the model without the inner orifice, $\rho=0$, is a universal one, as it contains no parameters.

We also considered a model with the nonlinearity switched to self-repulsion, i.e., $g(r)<0$, in the regions of $r<\rho$ and $r>R$. However, we focus on the case with $g=0$ in these regions, as such a case is least favorable for the existence of solitons, hence it provides for results which are most relevant to the experimental realization of the scheme.

Stationary solutions for fundamental solitons are looked for as $\psi=\phi(r)e^{-i\mu t}$, with a real chemical potential μ, and a real function ϕ obeying the equation

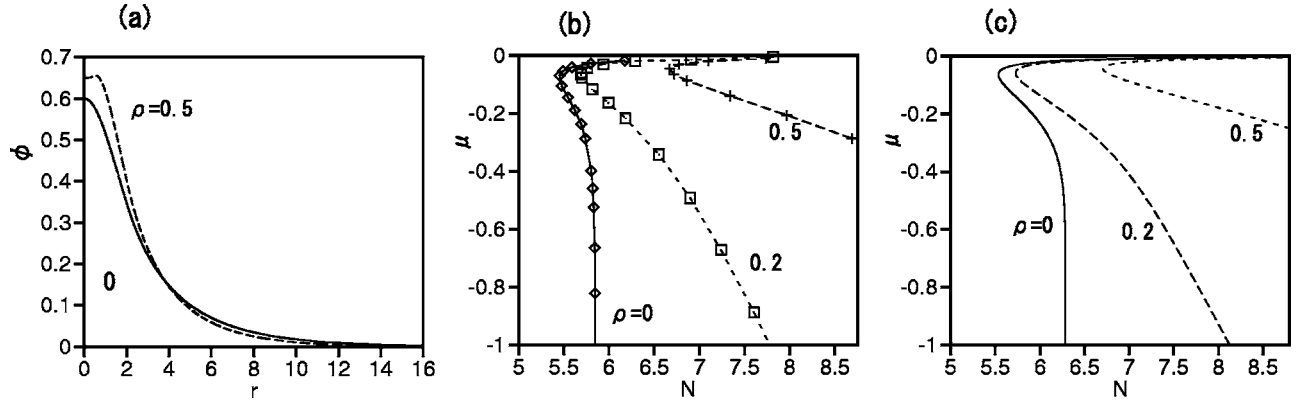

FIG. 1. (a) Examples of stable soliton solutions with $\rho=0$, $\mu=-0.0399$, and $N=5.59$ (solid curve) and $\rho=0.5$, $\mu=-0.0648$, and $N=6.721$ (dashed curve). (b) Chemical potential μ vs norm N for soliton families found numerically with $\rho=0$, 0.2, and 0.5. For $\rho=0$, the VK-stable portion of the solution, i.e., one with $dN/d\mu<0$, is found in the interval $N_{\rm cr}^{\rm (lower)}\approx 5.449<N<N_{\rm Townes}\approx 5.85$. (c) $\mu(N)$ curves predicted by the variational approximation for the same cases, $\rho=0$, 0.2, and 0.5.

$$2\mu\phi+\phi''+r^{-1}\phi'+2g(r)\phi^3=0 \tag{4}$$

(the prime stands for d/dr). Equation (4) is to be solved with the boundary conditions $\phi'(r=0)=0$ and $\phi(r=\infty)=0$ (the latter one implies that μ must be negative). The solution was searched for numerically by selecting the value of $\phi(r=0)$ with which the boundary condition at $r=\infty$ could be met.

Two examples of the solution are displayed in Fig. 1(a), one for $\rho=0$, i.e., the configuration with no inner "hole," and the other one with the "hole" corresponding to $\rho=0.5$; in the latter case, the solution attains a maximum at $r=\rho$, having a shallow minimum at $r=0$. Families of the soliton solutions are characterized by dependences $\mu(N)$, which are displayed in Fig. 1(b) for $\rho=0$ and two nonzero values of ρ. These dependences predict a necessary stability condition as per the VK criterion [33], $dN/d\mu<0$, i.e., parts of the solution families beneath the turning points in Fig. 1(b) may be stable (below, the turning point will be denoted as $N=N_{\rm cr}^{\rm (lower)}$). In fact, the stability region exists due to the fact that the attractive nonlinearity acts in a finite region of space $r<R$.

In the absence of the inner orifice ($\rho=0$), the soliton becomes narrow as μ takes large negative values. In this case, the medium seems nearly uniform for the soliton, hence it approaches the shape of the well-known Townes soliton, which is a universal weakly unstable localized solution of the 2D nonlinear Schrödinger (NLS) equation with the spatially uniform self-focusing nonlinearity [34]. Accordingly, the soliton's norm approaches the value $N_{\rm Townes}\approx 5.85$, which plays a critical role in the radial dynamics, being equal to the norm of the Townes soliton.

B. Variational approximation

The fundamental soliton solutions in the present model can also be obtained by means of the variational approximation (see a review of the method in Ref. [35]). To this end, we adopt the ansatz

$$\phi=A\exp\left(-\frac{r^2}{2w^2}\right), \tag{5}$$

with an amplitude A and width w. The substitution of the ansatz in norm (3) and the Lagrangian of Eq. (4),

$$L=2\pi\int_0^\infty\left[2\mu\phi^2-\left(\frac{d\phi}{dr}\right)^2+g(r)\phi^4\right]rdr, \tag{6}$$

yields $N=\pi A^2w^2$ (we use this relation to eliminate A in favor of N), and

$$L=2\mu N-\frac{N}{w^2}+\frac{N^2}{2\pi w^2}\left(1-e^{-2R^2/w^2}\right).$$

Then, the variational equations $\partial L/\partial N=0$ and $\partial L/\partial w=0$ predict the following relations between the norm, width and chemical potential of the soliton:

$$\frac{2\pi}{N}=\left(1-2\frac{\rho^2}{w^2}\right)e^{-2\rho^2/w^2}-\left(1-2\frac{R^2}{w^2}\right)e^{-2R^2/w^2},$$

$$\mu w^2=1-\frac{N}{2\pi(e^{-2\rho^2/w^2}-e^{-2R^2/w^2})}. \tag{7}$$

The $\mu(N)$ dependence, predicted by Eq. (7), is shown in Fig. 1(c) for several values of ρ. It is consistent with the numerical results displayed in Fig. 1(b), although the variational approximation predicts somewhat larger values of N.

C. The narrow-ring model

The simple ansatz (5) cannot predict the shape of the solution with the local minimum at $r=0$, such as the one shown in Fig. 1(a) for $\rho\neq 0$. The minimum becomes deeper as the nonlinearity-supporting annulus narrows, which corresponds to $(R-\rho)/R\to 0$. As a limit form, one can take the GPE with the δ-functional nonlinearity support

$$i\frac{\partial\psi}{\partial t}=-\frac{1}{2}\nabla^2\psi-\delta(r-R)|\psi|^2\psi \tag{8}$$

[the coefficient in front of the δ function is scaled to be 1, see Eq. (2)]. By final rescaling, one can again set $R=2$ in Eq. (8), as was done above in Eq. (1), so as to cast Eq. (8) in a parameter-free form. It is relevant to mention that a BEC configuration in the form of a narrow ring was recently created in the experiment by means of an accordingly shaped magnetic trap [36].

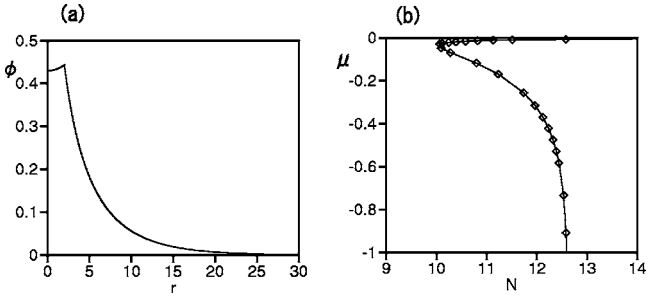

FIG. 2. (a) An example of the solution of Eq. (8). (b) The $\mu(N)$ dependence for the δ-functional model, according to Eq. (13).

In the present case, the stationary wave function $\phi(r)$ obeys a linear equation

$$\frac{d^2\phi}{dr^2} + \frac{1}{r}\frac{d\phi}{dr} + 2\mu\phi = 0, \tag{9}$$

which must be solved separately for $r<R$ and $r>R$. The inner and outer solutions, one with $\phi'(r=0)=0$ and the other vanishing at $r\to\infty$, are to be linked by the conditions of the continuity of $\phi(r)$ and jump of $\phi'(r)$ at $r=R$, which follows from Eq. (8):

$$\phi'(r=R+0) - \phi'(r=R-0) = -2[\phi(r=R)]^3. \tag{10}$$

Appropriate solutions to Eq. (9) are

$$\phi(r) = A\begin{cases} I_0(\sqrt{-2\mu}r)/I_0(\sqrt{-2\mu}R), & r<R, \\ K_0(\sqrt{-2\mu}r)/K_0(\sqrt{-2\mu}R), & r>R, \end{cases} \tag{11}$$

where I_0 and K_0 are the modified Bessel and Hankel functions, A is a constant, and the continuity of $\phi(r)$ at $r=R$ is provided automatically. The substitution of expressions (11) in Eq. (10) yields

$$A^2(\mu) = \sqrt{-\frac{\mu}{2}}\left[\frac{K_1(z)}{K_0(z)} + \frac{I_1(z)}{I_0(z)}\right]\Bigg|_{z=\sqrt{-2\mu}R}. \tag{12}$$

The norm (3) of the exact solution given by Eqs. (11) and (12) can also be calculated in an explicit form

$$N(\mu) = \pi\sqrt{-\frac{\mu}{2}}\left[\frac{K_1(z)}{K_0(z)} + \frac{I_1(z)}{I_0(z)}\right]\left[\frac{K_1^2(z)}{K_0^2(z)} - \frac{I_1^2(z)}{I_0^2(z)}\right]\Bigg|_{z=\sqrt{-2\mu}R}. \tag{13}$$

Figures 2(a) and 2(b) display, respectively, an example of the solution, and the $\mu(N)$ dependence plotted as per the exact expression (13).

D. Two-component solitons in the narrow-ring model

A binary BEC containing two different hyperfine states of one atomic species is described by a symmetric system of nonlinearly coupled GPEs [25–32]. It is natural to assume that the spatial modulation of the scattering length acts in the same way on the interaction in both components and between them. In particular, in the case of the nonlinearity concentrated at the narrow ring, the normalized coupled GPEs take the form [see Eq. (8)]

$$i\frac{\partial\psi_1}{\partial t} = -\frac{1}{2}\nabla^2\psi_1 - \delta(r-R)(|\psi_1|^2 + \sigma|\phi_2|^2)\psi_1, \tag{14}$$

$$i\frac{\partial\psi_2}{\partial t} = -\frac{1}{2}\nabla^2\psi_2 - \delta(r-R)(|\psi_2|^2 + \sigma|\psi_1|^2)\psi_2, \tag{15}$$

where, in the physically relevant situation, the "inter/intra" ratio of the scattering lengths is slightly larger than unity [22,25], $\sigma=1+\epsilon$, with $0<\epsilon\ll 1$ (the fact that $\sigma-1$ is positive and small has important implications for the existence and stability of 1D [27] and 2D [28] dynamical patterns in the binary BEC, in the form of domain walls that separate the two components).

A stationary vectorial-soliton solution to Eqs. (14) and (15) is looked for in the form of Eq. (11), with, generally, different chemical potentials μ_1 and μ_2 and different amplitudes A_1 and A_2 of wave functions $\psi_{1,2}=\phi_{1,2}(r)e^{-i\mu_{1,2}t}$. Then, straightforward consideration yields

$$A_{1,2}^2 = \frac{\sigma A^2(\mu_{2,1}) - A^2(\mu_{1,2})}{\sigma^2 - 1}, \tag{16}$$

where $A^2(\mu)$ is given by Eq. (12).

An essential condition is that both values $A_{1,2}^2$ given by Eqs. (16) must be positive. With regard to the fact that $\epsilon \equiv \sigma-1$ is small, it is easy to see that this condition is met if $\Delta\mu \equiv \mu_1-\mu_2$ is small too:

$$|\Delta\mu| < \epsilon A^2(\bar{\mu})/|[A^2(\bar{\mu})]'|, \tag{17}$$

where $\bar{\mu}\equiv(\mu_1+\mu_2)/2$, and the prime stands for the derivative with respect to $\bar{\mu}$. Expressions (16) then take the form

$$A_n^2 \approx \frac{1}{2}\left[A^2(\bar{\mu}) + (-1)^n[A^2(\bar{\mu})]'\frac{\Delta\mu}{\epsilon}\right]. \tag{18}$$

Note that, although the interval (17) of values of the chemical-potential difference, in which the vectorial soliton can be found, is narrow, within this interval the asymmetry of the soliton, which is measured by ratio A_1^2/A_2^2, taken as per Eqs. (18), is not restricted.

E. Stability diagram for stationary solitons

Figure 2(b) shows the existence of solutions with $dN/d\mu<0$ in the model with the radial δ function, which may be stable according to the VK criterion. However, it can only guarantee the stability against radial perturbations that do not break the axial symmetry of the solutions. On the other hand, it is well known that axisymmetric ring-shaped states may be easily subject to instability against azimuthal perturbations (see, e.g., Ref. [37]).

To study the stability against angular modulations in the general case [with $g(x)$ taken as per Eq. (2)], including the δ-functional limit, as in Eq. (8), we take a perturbed solution as

$$\psi(r,\theta,t) = e^{-i\mu t}[\phi(r) + \delta\phi_+(r)e^{-i\chi t+im\theta} + \delta\phi_-(r)e^{i\chi^* t-im\theta}], \tag{19}$$

where θ is the angular variable, m is an integer perturbation index, χ is a perturbation eigenfrequency, with * standing for

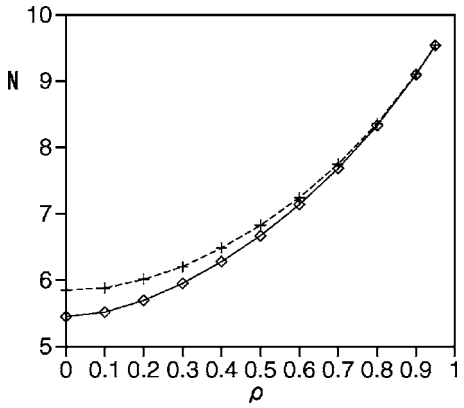

FIG. 3. The stability diagram for the soliton solutions. In the region between the two borders, the stationary solitons are stable—simultaneously according to the VK criterion, i.e., against radial perturbations (above the lower border) and against azimuthal modulations (below the upper border).

the complex conjugation (χ may be complex [37]), and $\delta\phi_{\pm}(r)$ are components of the respective eigenfunction. In particular, the instability threshold may correspond to $\chi=0$, then the eigenfunction has $\delta\phi_{+}=\delta\phi_{-}\equiv\delta\phi_{0}(r)$, and the substitution of expression (19) in Eq. (8) and subsequent linearization lead to an equation for the zero mode,

$$\left[\mu+\frac{1}{2}\left(\frac{d^2}{dr^2}+\frac{1}{r}\frac{d}{dr}-\frac{m^2}{r^2}\right)+3g(r)[\phi(r)]^2\right]\delta\phi_0=0. \tag{20}$$

The instability threshold is achieved when real μ, found as an eigenvalue of Eq. (20), coincides with the actual value of the chemical potential of the unperturbed solution $\phi(r)$. This way, the threshold was identified for the lowest azimuthal perturbation mode, with $m=1$ (in direct simulations presented in the next section, instability was observed solely against the azimuthal modulations with $m=1$).

The result of the analysis is summarized in Fig. 3, in the form of a stability diagram in the (ρ,N) parameter plane. The upper dotted border is the critical curve for the azimuthal instability with $m=1$, found as described above, while the lower dashed curve is the existence and stability border for the soliton solutions, which is identified as a set of turning points of the $\mu(N)$ curves in Fig. 1. Soliton solutions satisfying the VK criterion, $dN/d\mu<0$, exist above the lower border. Below the upper border, they are stable against the $m=1$ azimuthal disturbances, i.e., the solitons are expected to be completely stable between the two curves. This expectation was verified by direct simulations, see the next section.

Note that the border of the azimuthal instability in Fig. 3 is located, for $\rho=0$, at a value of N which is identical to $N_{\text{Townes}}\approx 5.85$, i.e., in the case of $\rho=0$ (no inner orifice), the thresholds for the collapse in the radial direction, and for the breakup of the axial symmetry in the azimuthal direction, are identical. The coincidence of the two thresholds for $\rho=0$ can be explained. Indeed, differentiation of Eq. (4) in r shows that, for given $\phi(r)$, the function $\phi'(r)$ solves the following linear equation:

$$\left[2\mu+\frac{d^2}{dr^2}+\frac{1}{r}\frac{d}{dr}-\frac{1}{r^2}+6g(r)[\phi(r)]^2\right]\phi'=-2g'(r)[\phi(r)]^3. \tag{21}$$

If $g'=0$, Eq. (21) exactly coincides with Eq. (20) for $m=1$, hence the function $\phi'(r)$ may be identified as the corresponding zero mode. Of course, when g is a function of x defined by Eq. (2), which means $g'(x)=\delta(r-R)$, the term on the right-hand side of Eq. (21) does not allow $\phi'(x)$ to be the zero mode; nevertheless, in the limit of $N\to N_{\text{Townes}}$, the soliton shrinks to a size much smaller than R, hence $[\phi(R)]^3$ becomes vanishingly small, along with the abovementioned term. Thus, in the limit of $N=N_{\text{Townes}}$, the function $\phi'(r)$ provides for a solution to Eq. (20) with $m=1$, making $N=N_{\text{Townes}}$ the threshold of instability to the azimuthal perturbations with $m=1$.

A notable feature of the stability diagram in Fig. 3 is that the lower and upper stability borders meet and close down the stability region at $\rho=\rho_{\max}\approx 0.95$, which means that the nonlinearity-carrying annulus with the ratio of the inner and outer radii exceeding the critical value $\rho_{\max}/R\approx 0.47$, cannot support stable solitons. This conclusion implies that solitons cannot be stable either in model (8) with the radial δ function. Indeed, detailed consideration of that model reveals the region of the azimuthal stability at $N>11.0$ and $\mu>-0.0116$, which entirely belongs to the upper branch of the $\mu(N)$ curve in Fig. 2(b), with $dN/d\mu>0$, i.e., the region is VK unstable.

III. DIRECT SIMULATIONS

To check the predictions for the stability of the solitons, and examine the evolution of unstable ones, we have performed direct 2D simulations by dint of the split-step Fourier method, employing a basis composed of 512×512 modes. The size of the integration domain was $L\times L=60\times 60$, with the center of the circle or annulus set at point $(x,y)=(L/2,L/2)$, and the time step $\Delta t=0.005$.

The simulations have confirmed the stability of the solitons in the region between the lower and upper borders in Fig. 3, and instability outside of this region. Figure 4(a) displays an example of the time evolution of $|\psi(x,L/2)|$ (i.e., the profile of the cross section through the central point along the x axis) in a perturbed stable soliton, for $\rho=0$. On the other hand, Figs. 4(b) and 4(c) demonstrate that (for the same case of $\rho=0$) unstable solitons suffer collapse.

However, unstable solitons [ones belonging to the upper, VK unstable, part of the $\mu(N)$ curve in Fig. 1(b), with $dN/d\mu>0$] whose norm is taken below a critical value $N_{\text{cr}}^{(\text{upper})}\approx 5.99$ (for $\rho=0$) which is *higher* than the norm $N_{\text{Townes}}\approx 5.85$ of the Townes soliton in the two-dimensional NLS equation, neither collapse nor decay into radiation (in the NLS equation, a pulse with $N<N_{\text{Townes}}$ is bound to decay in the 2D uniform space). Instead, the unstable soliton rearranges itself into a stable breather. Figures 5(a) and 5(b) display an example of the evolution of breathers. In the simulations, the breathers remain stable indefinitely long, their oscillations getting more regular as N decreases. The

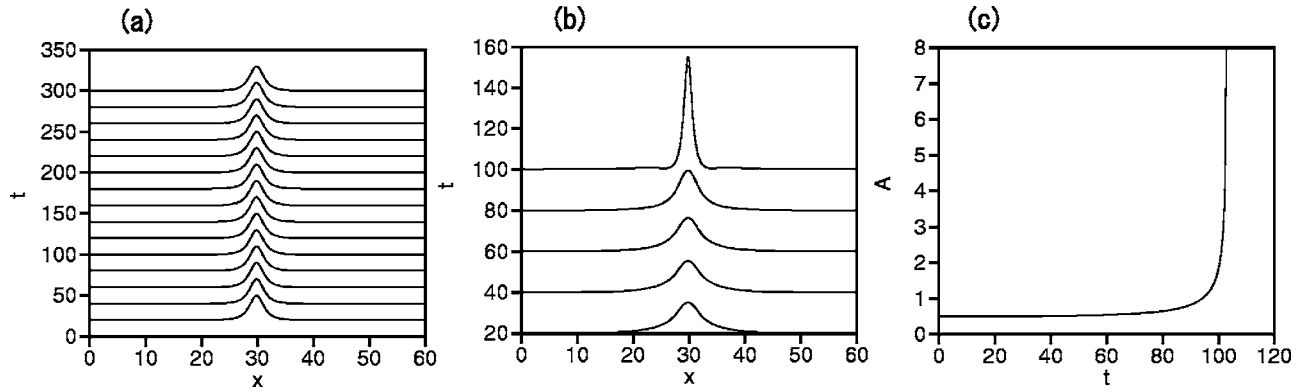

FIG. 4. (a) The evolution of $|\psi(x,L/2)|$ (central cross section) in a stable soliton for $\rho=0$, $\mu=-0.189$, and $N=5.62$. (b) An example of collapse of an unstable soliton, for $\rho=0$, $\mu=-0.0179$, and $N=6.175$. (c) The time dependence of the field amplitude, i.e., maximum value of $|\phi(x,y)|$, for the same case as in (b).

amplitude of the oscillations, which we define as the root-mean square of the variation of the soliton's amplitude $A(t)\equiv|u(x=y=L/2,t)|$ decreases with N, and it vanishes at another critical value $N_{\rm cr}^{\rm (lower)}\approx 5.449$. Up to the numerical accuracy, the latter one is precisely the smallest value of N at which the stationary solitons exist for $\rho=0$, see Fig. 1(b). Thus, $N=N_{\rm cr}^{\rm (lower)}$ is not only the point of the merger of the VK-stable and VK-unstable branches of the solutions, but also the one at which the breathers merge into the static solitons.

We stress that the existence of the stable axisymmetric breathers up to $N_{\rm cr}^{\rm (upper)}\approx 5.99$ does not contradict the fact that the symmetry-breaking azimuthal instability occurs, for $\rho=0$, at $N>N_{\rm Townes}\approx 5.85$, as explained above. Indeed, the latter pertains to the angular instability of the static solitons, but not breathers.

A noteworthy consequence of these results is the bistability: in the entire interval of values of the norm $N_{\rm cr}^{\rm (lower)}\approx 5.449<N<N_{\rm Townes}\approx 5.85$, where stable stationary solitons are found (for $\rho=0$), they coexist with breathers. On the other hand, in the adjacent interval $5.85<N<N_{\rm cr}^{\rm (upper)}\approx 5.99$, only stable breathers are possible (and no stable objects exist for $N>5.99$).

Stable breathers and bistability were found for $\rho>0$ as well. We note that stable breathers were also found in the model based on the one-dimensional GPE with a nonlinear OL [i.e., the nonlinearity coefficient modulated in space as $\cos(kx)$] [15]. In the latter model, bistability was observed too, as the breathers exist at the same values of the norm at which stable stationary solitons are found.

As said above, all the solitons which are stable against collapse in the model with $\rho=0$, are stable too against the azimuthal perturbations. Actual instability against the azimuthal mode (19) with $m=1$ occurs at $\rho>0$. To study the azimuthal instability in direct simulations, we used an initial condition in the form of a stationary soliton subjected to a weak angular deformation. Figure 6 displays a typical example of the development of the azimuthal instability for $\rho=0.55$. As a result, the soliton does not split into fragments, which is a generic result of the azimuthal instability of vortex-ring solitons in uniform media [36], but rather shifts from the central point $(x,y)=(30,30)$, to a position centered at $(x,y)\approx(29,30)$. Because the norm of the soliton exceeds $N_{\rm Townes}$, it then develops intrinsic collapse at the new position, where the hole does not essentially affect its dynamics. The shift of the soliton off the center and subsequent collapse were found to be a generic outcome of the development of the azimuthal instability. This feature can be easily explained by the fact obvious in Fig. 3: all the solitons which are subject to the azimuthal instability have $N>N_{\rm Townes}$, hence they

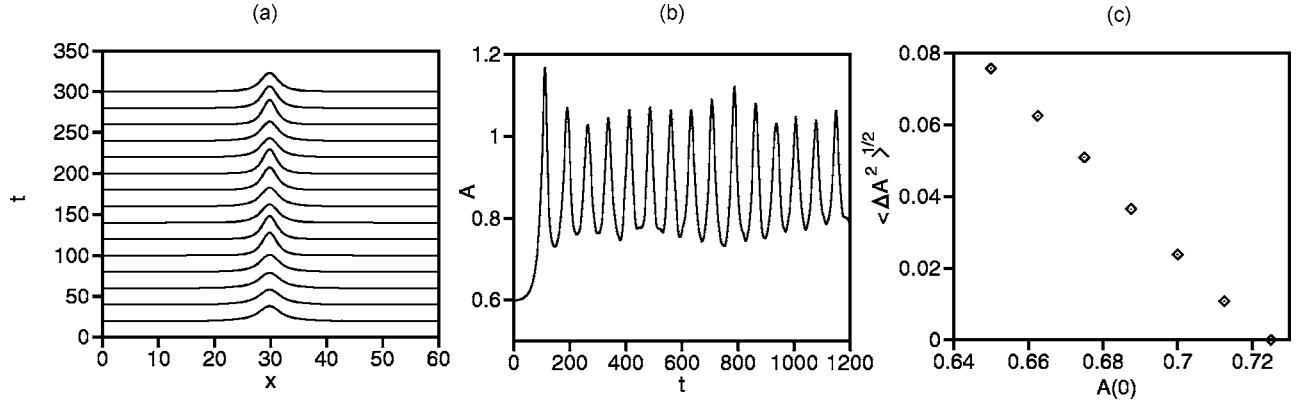

FIG. 5. (a) The time evolution of the cross-section profile $|\psi(x,L/2)|$ of a breather, for $\rho=0$, $\mu=-0.0399$, and $N=5.59$. The initial amplitude of the soliton is $A(0)=0.6$. (b) Evolution of the amplitude of the breathing soliton for the same case. (c) The amplitude of intrinsic oscillations of the breather as a function of $A(0)$.

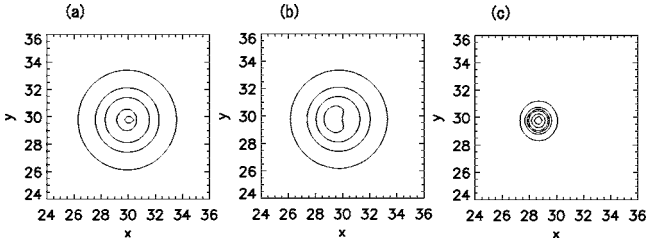

FIG. 6. Snapshots of contour maps of $|\psi(x,y)|$ for an azimuthally unstable soliton, taken at $t=5$ (a), $t=100$ (b), and $t=122$ (c). In this case, $\rho=0.55$, $\mu=-0.0782$, and $N=7.055$.

should collapse after being displaced away from the hole.

As said above, direct simulations corroborate the stability of the stationary solitons in the region between the two borders in Fig. 3. We illustrate this conclusion in Fig. 7, which displays the time evolution of the field amplitude [maximum value of $|\psi(x,y)|$] for $\rho=0.2$ and three different values of the norm. The first soliton, with $N=5.702$, belongs to the stability region in Fig. 3, and it is seen to be stable indeed. Two other solitons, with $N=5.994$ and $N=6.01$, are azimuthally unstable, which eventually leads to the collapse (after the spontaneous off-center shift, as shown in Fig. 6). Note that, as $N=5.994$ is close to the border of the azimuthal instability, the respective instability development time is large.

IV. VORTEX SOLITONS

In addition to the fundamental solitons considered above, Eq. (1) also gives rise to vortex solitons, in the form of $\psi=\phi_S(r)e^{-i\mu t+iS\theta}$, with integer vorticity S and real function $\phi(r)$ satisfying the equation [see Eq. (4)]

$$\phi_S'' + r^{-1}\phi_S' - S^2 r^{-2}\phi_S + 2g(r)\phi_S^3 + 2\mu\phi_S = 0. \qquad (22)$$

In particular, in the model with the radial δ function, see Eq. (8), the vortex solution can be found in an exact form, see Eqs. (11) and (12):

$$\phi_S(r) = A\begin{cases} I_S(\sqrt{-2\mu}r)/I_S(\sqrt{-2\mu}R), & r<R, \\ K_S(\sqrt{-2\mu}r)/K_S(\sqrt{-2\mu}R), & r>R, \end{cases}$$

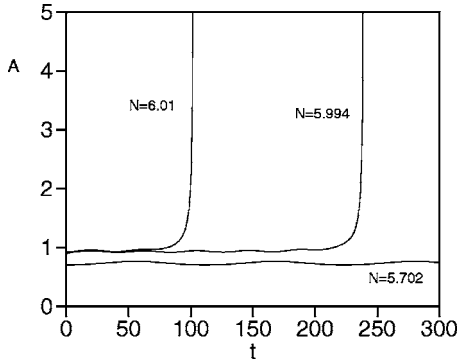

FIG. 7. The field amplitude vs time for weakly perturbed solitons with $\rho=0.2$ and (a) $N=5.702$, $\mu=-0.0758$, (b) $N=5.994$, $\mu=-0.164$, and (c) $N=6.01$, $\mu=-0.169$.

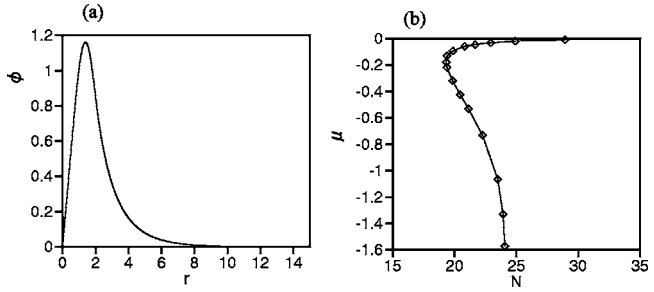

FIG. 8. (a) A typical example of profile $\phi(r)$ for the vortex soliton with $\rho=0$, $S=1$, and $N=23.9$, $\mu=-1.33$. (b) The $\mu(N)$ dependence for the vortex-soliton family with $\rho=0$ and $S=1$.

$$A^2 = \frac{1}{2}\sqrt{-\frac{\mu}{2}}\left[\frac{I_{S+1}(x)+I_{S-1}(x)}{I_S(x)} + \frac{K_{S+1}(x)+K_{S-1}(x)}{K_S(x)}\right]\Bigg|_{x=\sqrt{-2\mu}R}.$$

The norm of this solution can also be calculated in an analytical form.

An example of a vortex soliton, and the dependence $\mu(N)$ for these solutions, are displayed in Figs. 8(a) and 8(b), for $\rho=0$ and $S=1$. The figures show that a part of the solution family has $dN/d\mu<0$, hence it is stable against radial perturbations, pursuant to the VK criterion.

Comparing Fig. 8(b) to Fig. 1(b), one observes that the norm of the vortices is much larger than the norm of the fundamental solitons, which suggest that the vortex soliton may break up into a set of fundamental ones (as said above, this is a typical outcome of the development of azimuthal instability of vortex solitons in uniform media [36]). Indeed, further analysis demonstrates that the vortex solitons with $S=1$ are unstable against azimuthal disturbances with $m=2$ [see Eq. (19)]. An example, displayed in Fig. 9 for $\rho=0$, shows that the instability splits the vortex into a set of two zero-vorticity solitons, each then collapsing intrinsically, as its norm exceeds the critical value $N_{\text{Townes}}\approx 5.85$. Before the collapse, the soliton pair rotates in the counterclockwise direction. No example of a stable vortex soliton was found in the model.

V. CONCLUSION

The purpose of the work was to investigate the two-dimensional Gross-Pitaevskii equation in which the attrac-

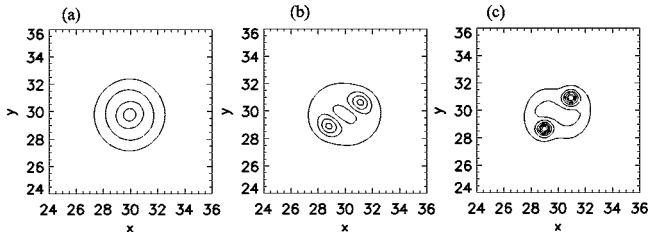

FIG. 9. Instability of vortex solitons is illustrated by a set of three snapshots of the contour map of $|\psi(x,y)|$ for a vortex with $S=1$, $\rho=0$, $N=23.9$, and $\mu=-1.33$, taken at $t=50$ (a), 85 (b), and 90 (c).

tive nonlinearity is limited to a finite region in the form of a circle or annulus, including the case of a narrow ring. In Bose-Einstein condensates trapped between a pair of blue-detuned light sheets, this configuration can be implemented through the Feshbach resonance by means of a properly configured dc magnetic, optical or electric field which controls the scattering length of collisions between atoms. Using numerical and analytical methods, we have found a stability region for axisymmetric fundamental (zero vorticity) solitons in the model, which is impossible in the case of the spatially uniform nonlinearity. It is noteworthy that the stability borders of the solitons in the model with the nonlinearity supported on the circle are completely determined by radial perturbations, while in the annular model the upper stability border is set by azimuthal modulations. The stability is limited to relatively broad annuli, with the ratio of the inner and outer radii smaller than a critical value $\rho_{\max}/R \approx 0.47$ (unstable solitons supported by the infinitely narrow ring were found in an exact form, including such solitons in the two-component model). Moreover, the model gives rise to bistability, as the stationary solitons coexist with stable axisymmetric breathers. The stability region of the breathers extends, in terms of their norm, to values exceeding the critical value corresponding to the Townes soliton. The collapse threshold strongly increases with the radius of the inner hole. Vortex solitons were constructed too, but they are unstable. Essentially the same results were obtained also for a model in which, outside of the circle or annulus, the nonlinearity is not zero but rather repulsive (that case is not explicitly considered in the paper, since the configuration with the zero nonlinearity is the most challenging one, as concerns the stability of solitons). The results reported in this work suggest a straightforward possibility to create stable two-dimensional matter-wave solitons in Bose-Einstein condensates.

ACKNOWLEDGMENTS

We acknowledge valuable discussions with D. Frantzeskakis and P. G. Kevrekidis. B.A.M. appreciates hospitality of the Department of Applied Science for Electronics and Materials at the Interdisciplinary Graduate School of Engineering Sciences, Kyushu University (Fukuoka, Japan). This work was partly supported by the Grant-in-Aid for Scientific Research No. 17540358 from the Ministry of Education, Culture, Sports, Science and Technology of Japan, and by the Israel Science Foundation through the Center-of-Excellence in Research Grant No. 8006/03.

[1] S. Burger, K. Bongs, S. Dettmer, W. Ertmer, K. Sengstock, A. Sanpera, G. V. Shlyapnikov, and M. Lewenstein, Phys. Rev. Lett. **83**, 5198 (1999); J. Denschlag, J. E. Simsarian, D. L. Feder, C. W. Clark, L. A. Collins, J. Cubizolles, L. Deng, E. W. Hagley, K. Helmerson, W. P. Reinhardt, S. L. Rolston, B. I. Schneider, and W. D. Phillips, Science **287**, 97 (2000).

[2] L. Khaykovich, F. Scherck, G. Ferrari, T. Bourdel, J. Cubizolles, L. D. Carr, Y. Castin, and C. Salomon, Science **296**, 1290 (2002); K. E. Strecker, G. B. Partridge, A. G. Truscott, and R. G. Hulet, Nature (London) **417**, 153 (2002).

[3] B. Eiermann, Th. Anker, M. Albiez, M. Taglieber, P. Treutlein, K.-P. Marzlin, and M. K. Oberthaler, Phys. Rev. Lett. **92**, 230401 (2004).

[4] J. M. Gerton, D. Strekalov, I. Prodan, and R. G. Hulet, Nature (London) **408**, 692 (2000); E. A. Donley, N. R. Claussen, S. L. Cornish, J. L. Roberts, E. A. Cornell, and C. E. Wieman, *ibid.* **412**, 295 (2001).

[5] B. B. Baizakov, B. A. Malomed, and M. Salerno, Europhys. Lett. **63**, 642 (2003); J. Yang and Z. Musslimani, Opt. Lett. **23**, 2094 (2003).

[6] B. B. Baizakov, B. A. Malomed, and M. Salerno, Phys. Rev. A **70**, 053613 (2004); B. B. Baizakov, M. Salerno, and B. A. Malomed, in *Nonlinear Waves: Classical and Quantum Aspects*, edited by F. Kh. Abdullaev and V. V. Konotop (Kluwer Academic, Dordrecht, 2004), p. 61; also available at http://rsphy2.anu.edu.au/~asd124/Baizakov_2004_61_NonlinearWaves.pdf

[7] H. Sakaguchi and B. A. Malomed, Europhys. Lett. **72**, 698 (2005).

[8] P. Pedri and L. Santos, Phys. Rev. Lett. **95**, 200404 (2005).

[9] S. Inouye, M. R. Andrews, J. Stenger, H.-J. Miesner, D. M. Stamper-Kurn, and W. Ketterle, Nature (London) **392**, 151 (1998); E. A. Donley, N. R. Claussen, S. L. Cornish, J. L. Roberts, E. A. Cornell, and C. E. Wieman, *ibid.* **412**, 295 (2001); H. Saito and M. Ueda, Phys. Rev. A **65**, 033624 (2002).

[10] P. G. Kevrekidis, G. Theocharis, D. J. Frantzeskakis, and B. A. Malomed, Phys. Rev. Lett. **90**, 230401 (2003).

[11] H. Saito and M. Ueda, Phys. Rev. Lett. **90**, 040403 (2003); F. Kh. Abdullaev, J. G. Caputo, R. A. Kraenkel, and B. A. Malomed, Phys. Rev. A **67**, 013605 (2003); G. D. Montesinos, V. M. Pérez-García, and P. J. Torres, Physica D **191**, 193 (2004).

[12] M. Trippenbach, M. Matuszewski, and B. A. Malomed, Europhys. Lett. **70**, 8 (2005); M. Matuszewski, E. Infeld, B. A. Malomed, and M. Trippenbach, Phys. Rev. Lett. **95**, 050403 (2005).

[13] P. O. Fedichev, Yu. Kagan, G. V. Shlyapnikov, and J. T. M. Walraven, Phys. Rev. Lett. **77**, 2913 (1996).

[14] M. Theis, G. Thalhammer, K. Winkler, M. Hellwig, G. Ruff, R. Grimm, and J. H. Denschlag, Phys. Rev. Lett. **93**, 123001 (2004).

[15] H. Sakaguchi and B. A. Malomed, Phys. Rev. E **72**, 046610 (2005).

[16] F. Kh. Abdullaev and J. Garnier, e-print cond-mat/0511264.

[17] G. Fibich, Y. Sivan, and M. I. Weinstein, http://www.columbia.edu/miw2103/recentpub.html.

[18] G. Theocharis, P. Schmelcher, P. G. Kevrekidis, and D. J. Frantzeskakis, Phys. Rev. A **72**, 033614 (2005).

[19] M. Marinescu and L. You, Phys. Rev. Lett. **81**, 4596 (1998).

[20] Y. V. Kartashov, V. A. Vysloukh, and L. Torner, Phys. Rev. Lett. **93**, 093904 (2004); Y. V. Kartashov, V. A. Vysloukh, and L. Torner, *ibid.* **94**, 043902 (2005); Y. V. Kartashov, A. A.

Egorov, V. A. Vysloukh, and L. Torner, J. Opt. Soc. Am. B **6**, 444 (2004).

[21] A. Görlitz, J. M. Vogels, A. E. Leanhardt, C. Raman, T. L. Gustavson, J. R. Abo-Shaeer, A. P. Chikkatur, S. Gupta, S. Inouye, T. Rosenband, and W. Ketterle, Phys. Rev. Lett. **87**, 130402 (2001).

[22] C. J. Myatt, E. A. Burt, R. W. Ghrist, E. A. Cornell, and C. E. Wieman, Phys. Rev. Lett. **78**, 586 (1997); D. S. Hall, M. R. Matthews, J. R. Ensher, C. E. Wieman, and E. A. Cornell, *ibid.* **81**, 1539 (1998).

[23] P. Maddaloni, M. Modugno, C. Fort, F. Minardi, and M. Inguscio, Phys. Rev. Lett. **85**, 2413 (2000).

[24] G. Modugno, M. Modugno, F. Riboli, G. Roati, and M. Inguscio, Phys. Rev. Lett. **89**, 190404 (2002).

[25] H. Pu and N. P. Bigelow, Phys. Rev. Lett. **80**, 1130 (1998).

[26] R. Ejnisman, H. Pu, Y. E. Young, N. P. Bigelow, and C. K. Law, Opt. Express **2**, 330 (1998); M. Trippenbach, K. Goral, K. Rzazewski, B. Malomed, and Y. B. Band, J. Phys. B **33**, 4017 (2000).

[27] M. I. Merhasin, B. A. Malomed, and R. Driben, J. Phys. B **38**, 877 (2005).

[28] B. A. Malomed, H. E. Nistazakis, D. J. Frantzeskakis, and P. G. Kevrekidis, Phys. Rev. A **70**, 043616 (2004).

[29] D. Schumayer and B. Apagyi, Phys. Rev. A **69**, 043620 (2004); V. M. Perez-Garcia and J. B. Beitia, *ibid.* **72**, 033620 (2005).

[30] P. G. Kevrekidis, H. Susanto, R. Carretero-Gonzalez, B. A. Malomed, and D. J. Frantzeskakis, Phys. Rev. E **72**, 066604 (2005).

[31] A. Simoni, F. Ferlaino, G. Roati, G. Modugno, and M. Inguscio, Phys. Rev. Lett. **90**, 163202 (2003).

[32] G. D. Montesinos, V. M. Perez-Garcia, and H. Michinel, Phys. Rev. Lett. **92**, 133901 (2004).

[33] M. G. Vakhitov and A. A. Kolokolov, Izv. Vyssh. Uchebn. Zaved., Radiofiz. **16**, 1020 (1973) [Sov. J. Quantum Electron. **16**, 783 (1973)].

[34] L. Bergé, Phys. Rep. **303**, 260 (1998).

[35] B. A. Malomed, in *Progress in Optics*, edited by E. Wolf (North-Holland, Amsterdam, 2002), Vol. 43, p. 71.

[36] S. Gupta, K. W. Murch, K. L. Moore, T. P. Purdy, and D. M. Stamper-Kurn, Phys. Rev. Lett. **95**, 143201 (2005).

[37] I. Towers, A. V. Buryak, R. A. Sammut, B. A. Malomed, L. C. Crasovan, and D. Mihalache, Phys. Lett. A **288**, 292 (2001); a short review of the topic was given in B. A. Malomed, G. D. Peng, P. L. Chu, I. Towers, A. V. Buryak, and R. A. Sammut, Pramana, J. Phys. **57**, 1061 (2001).